A GEOMETRICAL MODEL FOR PLASMA MIRROR ALIGNMENT IN HIGH-POWER LASER EXPERIMENTS

Dmitrii Nistor[1,2*], Alexandru Măgureanu[1,2], Cătălin Mihai Ticoş[1,2]

Precise alignment of plasma mirrors (PMs) is critical in high-power laser experiments to ensure optimal temporal contrast and maximize the energy content of the reflected main laser pulse. This work presents a geometrical model designed to streamline PM alignment by accounting for key parameters such as beam diameter, pulse power, off-axis parabolic (OAP) mirror angle and focal length. The model distinguishes between minor and major axes of the laser beam spot on the PM surface, addressing their distinct dependencies on geometrical and optical factors. Through auxiliary geometrical constructs, we derived analytical expressions for distances governing the PM surface intensity distribution. The model allows for precise prediction of optimal PM placement and alignment, leading to experimental results that indicate the appropriate intensity level from the 1PW High-Power Laser System. This approach provides a robust framework for improving PM efficiency, enhancing experimental reliability, and safeguarding upstream laser components in high-intensity laser systems.

Keywords: high-power laser, femtosecond pulse, plasma-mirror, contrast, geometrical optics

1. Introduction

High-power laser systems have revolutionized the field of ultrafast physics, enabling experiments that probe the fundamental dynamics of matter on femtosecond timescales. As these systems reach petawatt power levels [1], their applications in areas such as particle acceleration [2], high-energy density physics [3], and secondary radiation generation [4] continue to expand. However, achieving optimal performance in such experiments requires precise control of laser parameters, particularly temporal contrast and energy delivery. Temporal contrast [5] defined as the ratio of the main pulse intensity to the background light including prepulses and pedestal of the main pulse is crucial

[1]Extreme Light Infrastructure - Nuclear Physics (ELI-NP), Horia Hulubei National Institute of Physics and Nuclear Engineering, 30 Reactorului St., Măgurele, Ilfov 077125, Romania, corresponding author: dmitrii.nistor@eli-np.ro

[2]Engineering and Applications of Lasers and Accelerators Doctoral School (SDIALA), National University of Science and Technology POLITEHNICA Bucharest, 313 Splaiul Independenţei St., Bucharest RO-060042, Romania

for the accuracy of ultra-high power experiments. Poor contrast can result in premature ionization of the target or its total destruction, adversely affecting the experimental outcomes.

One widely used solution to this challenge is the plasma mirror (PM), an optical element that takes advantage of the intensity-dependent reflectivity of an anti-reflective surface [6] to suppress the prepulse and pedestal light while reflecting the high-intensity main pulse towards the target. In addition to enhancing temporal contrast [7], a PM plays a vital role in attenuating back-reflected light from the experimental chamber [8], thereby protecting upstream laser components from potential damage. The effectiveness of a PM depends on its position and angle relative to the incoming laser beam. Too intense of an interaction leads to inefficient contrast cleaning [9] and possible wavefront distortions [10] due to plasma expansion. In contrast, insufficient intensity reduces the reflectivity, resulting in significant energy losses on the target. High-power laser facilities typically use a single PM or, for superior contrast enhancement, a double PM system [11, 12, 13, 14, 15, 16, 17]

In this work, our aim is to streamline PM alignment by providing a set of geometrical equations to estimate the precise intensity on the PM surface based on placement and setup parameters. A rendered representation of experimental geometry is represented in Figure 1. By incorporating key factors such as beam diameter, pulse power, and OAP mirror geometry, we conceived a generalized geometrical model designed to offer practical guidelines for optimizing PM performance in high-power laser systems.

2. **Theoretical model**

The development of an accurate geometrical model for PM placement requires a comprehensive analysis of all factors influencing the beam's interaction with the PM surface. A crucial parameter is the half-angle of the OAP relative to the incident beam, denoted as $\hat{o}$, which governs how the laser beam is distributed onto its surface. A larger OAP angle results in a longer ellipsoidal distribution, influencing the geometrical model, as shown in Fig. 1. This theoretical model assumes that the angles $\hat{o}$ and $\hat{\omega}$ are contained within the same plane, which is a common experimental geometry.

In the following, the curvature of the OAP is neglected and we approximate the OAP paraboloid with a plane [18]. The angle $\hat{\omega}$ generates its own ellipsoidal projection onto the PM within the same plane. To account for these geometric features, we divide our calculations into two components: the minor and major axes of the ellipsoidal beam profile on the PM surface, which are the two values needed to determine the surface S.

$$S = \pi \; d \; D, \tag{1}$$

where d and D are the radii corresponding to the minor and major axis of the ellipse, respectively. The minor axis $2d$ is independent of both the angles $\hat{o}$ and

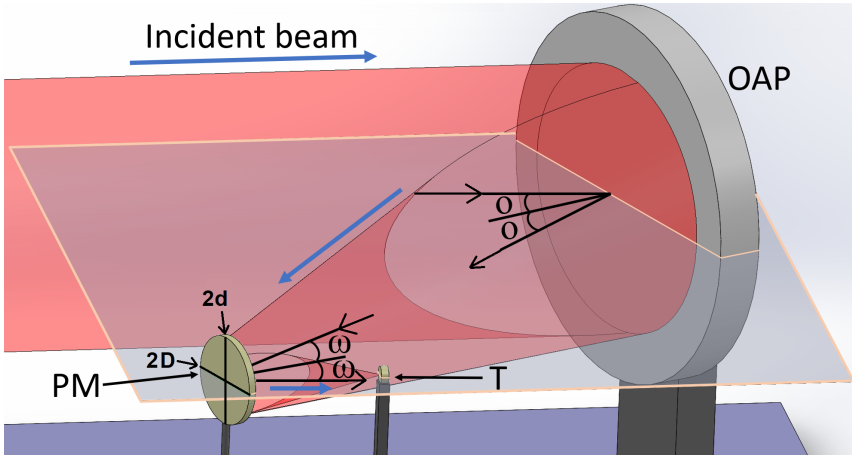

FIGURE 1. Rendered representation of the experimental setup. The incoming collimated beam is reflected off the OAP and focused onto the target via the PM. The minor and major axes of the ellipsoidal beam profile formed on the PM are denoted by d and D, respectively. The horizontal plane containing the OAP and PM half angles (i.e. $\hat{o}$ and $\hat{\omega}$, respectively) is highlighted and will be later utilized in Figure 2 to determine the theoretical model

$\hat{\omega}$. It depends solely on the distance x from the focal point, the effective focal length f, and the initial diameter of the laser beam Φ. This axis is determined by straightforward geometrical relationships involving these parameters [19] as follows:

$$d = \frac{\Phi x}{2f}. \tag{2}$$

The major axis $2D$, in contrast, is influenced by the entire set of parameters, including both $\hat{o}$ and $\hat{\omega}$. It is asymmetrical with respect to the central axis of beam propagation when $\hat{o}$ and $\hat{\omega}$ differ [14]. To calculate it, we split it across the beam's central axis, and break it into two geometric problems, solving for the length of segments i and j:

$$D = \frac{i + j}{2}. \tag{3}$$

A detailed geometrical model of the major axis and its dependencies is shown in Figure 2. Here, the OAP and PM are represented by straight blue and red lines, respectively. Additionally, the beam's trajectory following its interaction with the PM is shown behind the mirror, which is a standard representation in geometrical optics involving reflective surfaces. We consider that the OAP focuses the beam at its focal point F. To simplify the geometric analysis, we approximate the projection of the OAP surface onto the horizontal

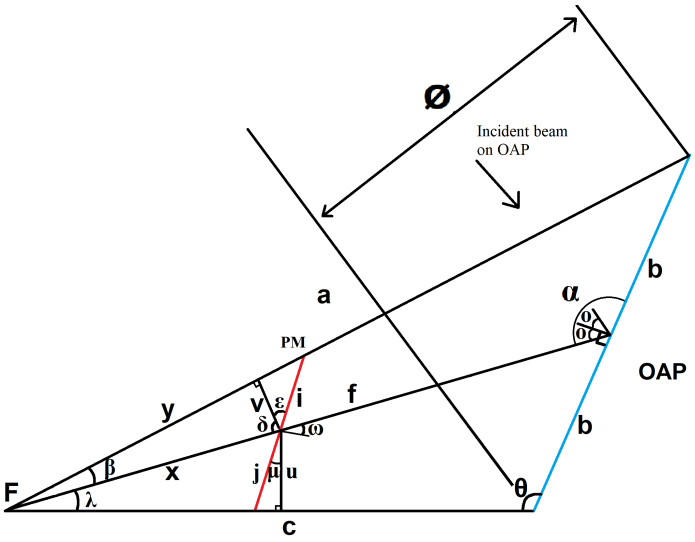

FIGURE 2. Geometrical model depicting the horizontal plane of major axis. Φ is the incident beam diameter on the OAP, PM is situated at a distance x from focal point F which is the position of the target. The effective focal length of OAP is f. The width of the incident laser spot on the OAP is $2b$.

TABLE 1. Known and to be determined (TBD) quantities.

Parameter	Description	Value
OAP effective focal length	f	67 cm
OAP off-axis angle	$2\hat{o}$	45°
Laser beam width (diameter)	2b	18 cm
Laser power	P	$\sim 10^{15}$ W
Intensity on PM	I	TBD (expect $\sim 1 - 6 \times 10^{15}$ W/cm^2)
Major laser diameter on PM	$2D = i + j$	TBD
Area of laser spot on PM	S	TBD
Distance between PM and F	x	TBD
Angle of PM	ω	TBD (constrained to $\sim 20 - 30°$)

plane as a line segment $2b$. This plane also coincides with the p-polarization of the laser beam. This approximation is justified by the relationships between the OAP's parameters such as the effective focal length f, the beam diameter Φ and off-axis angle $2\hat{o}$ and the features of the sphere which describe the curvature of the OAP, as we shall demonstrate in the next section.

Table 1 summarizes the key parameters used in the calculations, along with the quantities to be derived for organizing the setup.

Based on diameter Φ and $\hat{o}$ we determine the projection of the beam onto the OAP.

$$b = \frac{\Phi}{2\cos(\hat{o})}. \tag{4}$$

From f, b, and $\hat{\alpha}$ ($\hat{\alpha} = 90^\circ + \hat{o}$) we apply the cosine law to obtain the distance a:

$$a = \left[f^2 + b^2 - 2bf\cos(90^\circ + \hat{o})\right]^{1/2}. \tag{5}$$

Given that all sides a, b and f are known, we can now solve for $\hat{\beta}$ utilizing again the cosine law:

$$\cos(\hat{\beta}) = \frac{a^2 + f^2 - b^2}{2af}. \tag{6}$$

To aid in solving for i, we trace a line v from the intersection point between the PM and the beam central axis perpendicular to the side a. We employ this auxiliary geometrical construct which creates a right triangle with the sides x, y and v, needed to create relationships from the known input parameters: v can be easily deduced ($v = x\sin\hat{\beta}$), as well as the newly generated angle $\hat{\epsilon}$ ($\hat{\epsilon} = 90^\circ + \hat{\omega} - \hat{\delta}$, where $\hat{\delta} = 90^\circ - \hat{\beta}$). Now we can solve for i ($i = v/\cos\hat{\epsilon}$) and conclude the first half of the problem.

Similarly to i, we can calculate j and having a complete knowledge of the abf triangle we implicitly have information regarding $\hat{\lambda}$ ($\hat{\lambda} = \hat{\alpha} - \hat{\theta}$), $\hat{\theta}$ and c:

$$c = \left\{a^2 + 4b^2 - 4ab\cos\left[90^\circ - \arccos\left(\frac{a^2 + f^2 - b^2}{2af}\right) - o\right]\right\}^{1/2}, \tag{7}$$

where the argument of the cosine function in the above Eq. (7) is $180^\circ - \hat{\theta} - \hat{\lambda} - \hat{\beta} = 90^\circ - \hat{\beta} - \hat{o}$ and $\hat{\beta}$ is obtained from Eq. (6). With the knowledge of c we can calculate $\hat{\theta}$:

$$\hat{\theta} = \arccos\left(\frac{4b^2 + c^2 - a^2}{4cb}\right). \tag{8}$$

Tracing a line segment u from the intersection between PM and the central axis perpendicular to the side c gives a right triangle from which one can deduce u and j: $u = x\sin\hat{\lambda}$, $j = u/\cos\hat{\mu}$, where $\hat{\mu} = \hat{\epsilon} + \hat{\delta} - 90^\circ - \hat{\lambda}$ and furthermore $\hat{\mu} = 90^\circ + \hat{o} - \hat{\theta}$.

Building on these findings, the process of deriving a more generalized formula can be further streamlined. By incorporating all the geometric dependencies outlined above, several variables can be substituted to obtain a generalized expression for both i and j

$$i = \frac{x\sin\left[\arccos\left(\frac{a^2+f^2-b^2}{2af}\right)\right]}{\cos\left[\arccos\left(\frac{a^2+f^2-b^2}{2af}\right) + \hat{\omega}\right]}, \tag{9}$$

$$j = \frac{x \sin\left[90^\circ + \hat{o} - \arccos\left(\frac{4b^2+c^2-a^2}{4bc}\right)\right]}{\cos\left[\hat{\omega} - 90^\circ - \hat{o} + \arccos\left(\frac{4b^2+c^2-a^2}{4bc}\right)\right]}. \tag{10}$$

We also know the dependency between area S, laser power P and laser intensity I, where $S = P/I$. As such, we can enunciate a generalized formula for intensity on PM by replacing variables in Eq. 1:

$$\frac{P}{I} = \frac{\pi x \Phi (i + j)}{4f}, \tag{11}$$

where i, j, a, b, and c are given by Eqs. 9, 10, 5, 4 and 7, respectively.

By accounting for these geometrical particularities, the proposed model provides a generalized and robust framework for optimizing plasma mirror placement in high-power laser systems.

3. **Experiment**

We apply our model to the conditions and constraints of a real experimental setup that uses a 1 PW beam delivered by the High-Power Laser System (HPLS) at ELI-NP [20]. ELI-NP is a facility that can produce some of the most intense laser pulses in the world [21] with a peak power of 10 PW, allowing nuclear physics experiments to be carried out [22, 23]. In our experiment, the laser had an energy per pulse of 24 J and a pulse duration of about 24 fs. The purpose of the experimental campaign utilizing the 1 PW configuration was to irradiate different types of thin film targets for evaluating proton acceleration [24]. The specific setup configuration presented here enabled the acceleration of protons to cut-off energies of approximately 20–30 MeV using Al and DLC foils as targets, with thicknesses ranging from 0.16 to 3 microns.

The experimental setup involved a laser beam with a diameter of 180 mm focused by an OAP mirror which has a focal length f = 670 mm and is designed to operate for a deflection (or off-axis) angle $2\hat{o} = 45^\circ$, i.e. the angle between the incoming laser beam and the normal to the reflective surface is $\hat{o} = 22.5^\circ$, as given in Table 1 [25].

To verify the validity of the planar approximation of the OAP surface made in the previous section and in Figure 2, we determined the curvature of the vertex of the parent sphere (i.e., the sphere from which the OAP is derived) which is ≈ 114.4 cm [27]. Given that the PM is tilted at $\approx 39.7^\circ$ relative to the focal axis of this sphere, we inferred that the arc width subtended by the mirror on the sphere is 23.4 cm. This value closely matches the arc length of ≈ 23.44 cm, which corresponds to a subtended angle of 11.7°on the sphere. Thus, the arc length and the arc width are nearly identical, supporting the validity of the approximation.

The beam is reflected off the PM and then is focused on a target oriented at 17° relative to the incoming beam to mitigate intense back-scattering of light, as shown in Figure 3 [26].

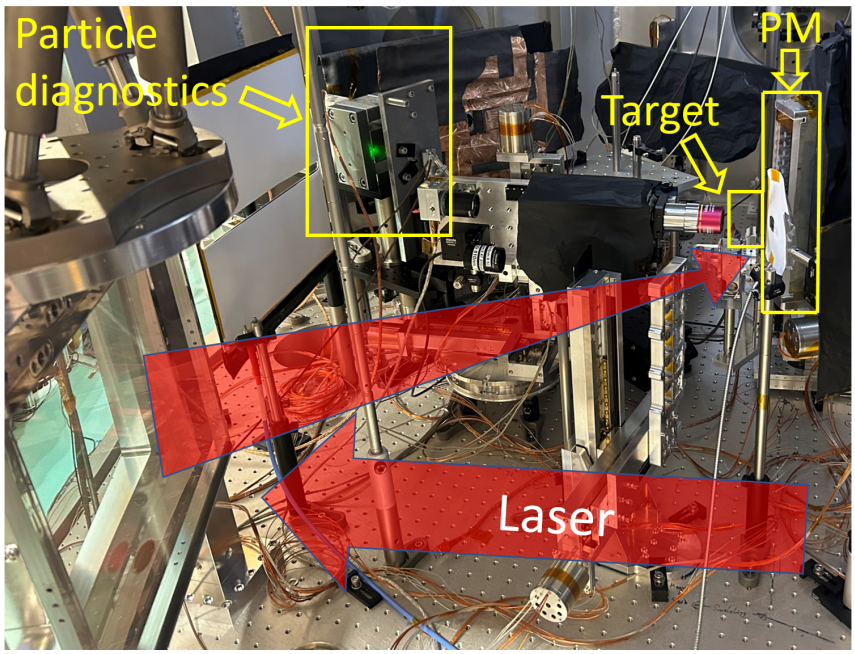

FIGURE 3. Setup with OAP, PM which consists of a AR coated glass slab and the target mounted on a support near the PM. The particle diagnostics were dedicated to proton detection

.

The PM consisted of an anti-reflective (AR) coated glass surface, placed at a distance $x \approx 3-6$ cm upstream of the target. The desired laser intensity for optimum performance of the PM was in the range $I = 1-6\times10^{15}$ W/cm^2 while operation at half-angle $\hat{\omega} \approx 20-30^\circ$ was dictated by the orientation of the particle diagnostics. The position and half-angle of the PM were crucial to meeting these specific requirements. Therefore, it was necessary to analyze the intensity as a function of both $\hat{\omega}$ and x. By replacing the variables in the generalized model given by Eq. (11) with our experimental parameters we obtain

$$\frac{P}{I} = 2.11\times10^{-3}x^2\left[\frac{0.1264}{\cos(7.25^\circ+\omega)}+\frac{0.1409}{\cos(\omega-8.1^\circ)}\right], \tag{12}$$

where x is given in cm. Using Eq. (12) we generate a 3D surface that highlights the dependency between intensity I, distance x, and angle $\hat{\omega}$ as shown in Figure 4. Furthermore, we can generate 2D plots to observe the evolution of intensity I with respect to distance x for fixed values of $\hat{\omega}$ as shown in Figure 5. Similarly, we can highlight the evolution of the intensity with $\hat{\omega}$ for specific distances x as shown in Figure 6.

The presented maps can be used to infer the evolution of parameters between different physical experimental setups and constraints. Figure 4 illustrates the relationship between PM position, angle, and intensity, highlighting

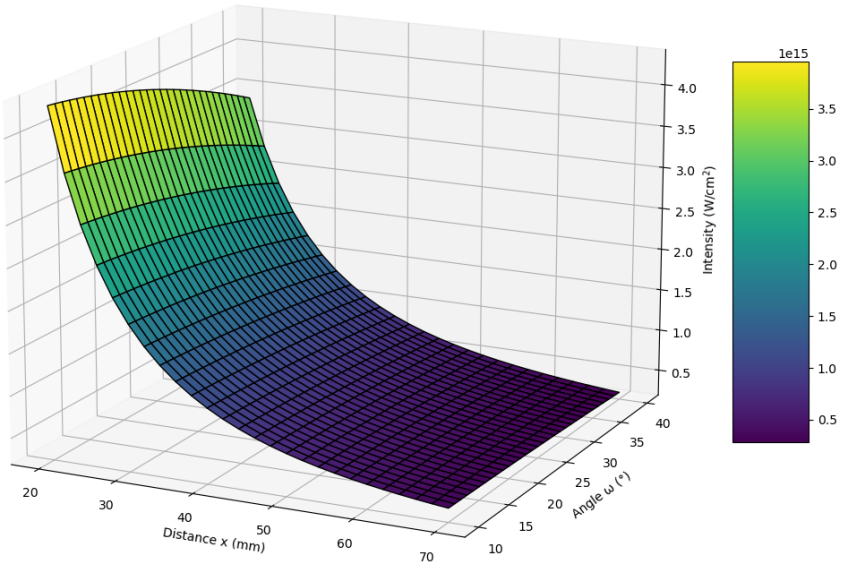

FIGURE 4. 3D surface highlighting dependencies between intensity I on PM, position x and angle $\hat{\omega}$.

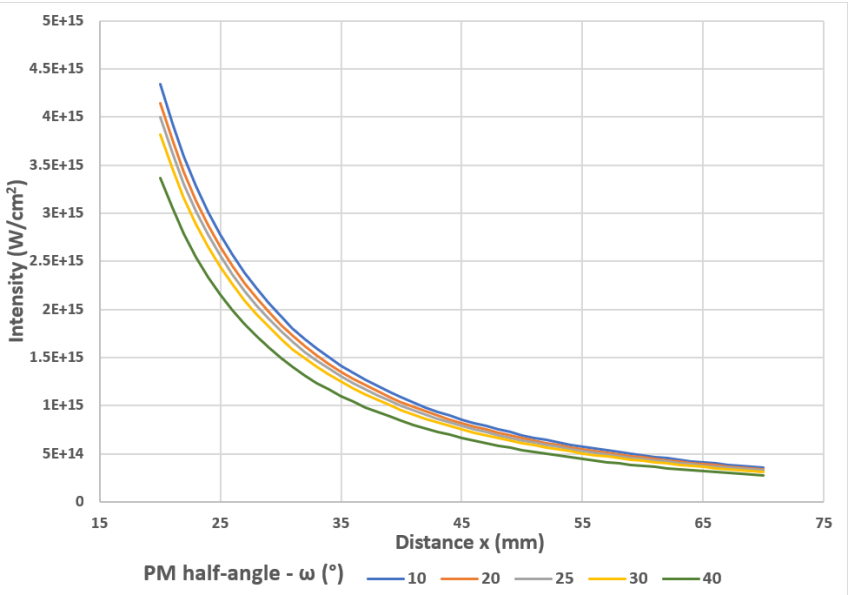

FIGURE 5. 2D map highlighting the dependency between intensities on PM I and position x for fixed $\hat{\omega}$ angles.

critical alignment parameters. The analysis of Figure 6 reveals that intensity varies nonlinear and slowly with the PM angle $\hat{\omega}$, while Figure 5 presents the rapid rise of intensity when the distance x is shortened. This is because the angle influences only the major axis of the ellipse on the PM, whereas the position influences both the minor and major axes. Moreover, slices of the 3D

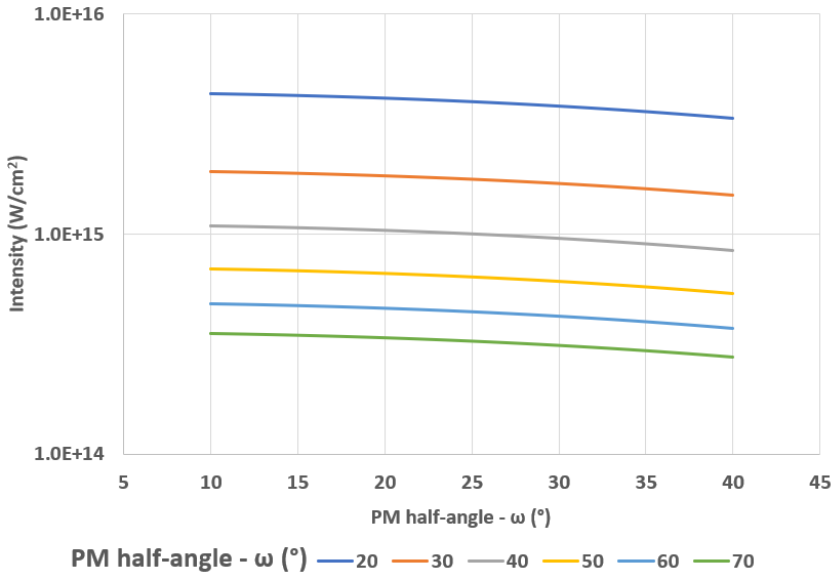

FIGURE 6. 2D map highlighting the dependency between intensities on PM I and half-angle $\hat{\omega}$ for fixed distances x.

surface can be plotted with x as a function of $\hat{\omega}$ for fixed desired intensities as seen in Figure 7. This systematic approach allows for precise predictions of the ellipsoidal beam profile on the PM surface, a critical factor in achieving the desired intensity range for effective temporal contrast enhancement and back-reflection attenuation.

The theoretical results given by Eq. (12) need to be corroborated with the previous measurements of PM reflectivity, which was around 75%, as well as the optimized contrast of 10^{-10} at -20 ps, as reported in [28] and [29], respectively. Note that these values reported in [28] and [29] were measured for an identical setup geometry and for the same OAP and PM type, thus validating their use here.

4. Conclusion

We have presented a generalized geometrical model that estimates the area of the laser beam spot and implicitly its intensity on a PM based on the parameters composing the experimental setup, such as laser beam diameter and power as well as the OAP half-angle and focal length. The generalized model was derived by simplifying some geometrical particularities which do not affect the final result, splitting the problem into two parts according to the symmetry around the central axis of the beam. Although the model functions accurately, it is just one of many possible approaches. Various strategies can be used to calculate the surface of the ellipse forming on the PM, employing different simplifications, auxiliary geometric constructs, and fundamental geometric theorems.

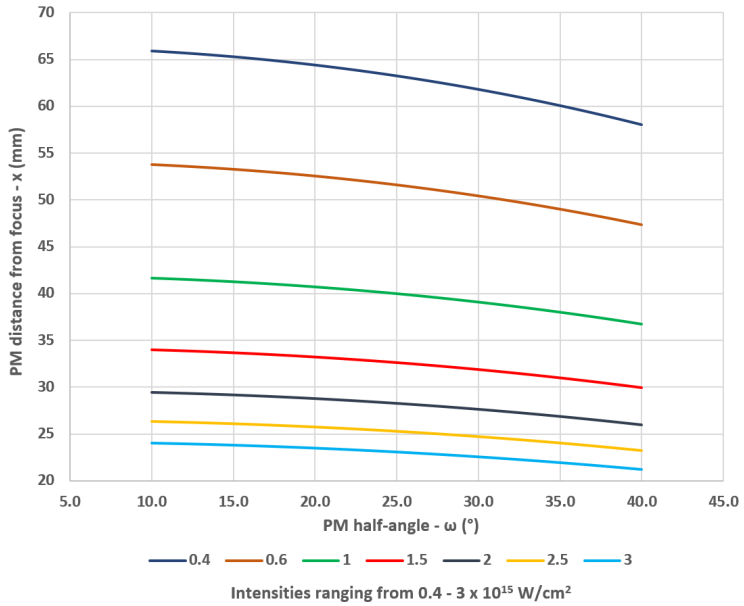

FIGURE 7. Map of dependencies between position x and angle $\hat{\omega}$ for specific intensities I on the PM.

Using this model, we applied the specific parameters of our laser and experimental setup to develop a guideline for the placement and alignment of the PM. Although the model presents the intensity on the PM, it overlooks the physical dimensions of the target and target mount, which could eclipse the beam traveling from the OAP onto the PM for a sufficiently small x and $\hat{\omega}$. Based on the information provided by the map and the physical constrains of our setup, we have utilized the PM at a half-angle $\hat{\omega} = 22.5°$ positioned at $x = 30$ mm from the focus to achieve a desired intensity of $I \approx 1.8 \times 10^{15}\ W/cm^2$. This model offers a reliable and practical tool for optimizing PM alignment, contributing to more efficient and accurate high-power laser[29]experiments.

Acknowledgments

This work was supported by the PN 23 21 01 05 contract sponsored by the Romanian Ministry of Research, Innovation and Digitalization, the IOSIN funds for research infrastructures of national interest, the IMPULSE project funded by the EU's Horizon 2020 research and innovation program under grant agreement No 871161 and project ELI-RO-19 "HighProton- PLas" funded by IFA.

REFERENCES

[1] *D. Strickland and G. Mourou*, Compression of amplified chirped optical pulses, Opt. Commun. **55**(1985), 447-449.

[2] *P. Norreys*, Laser-driven particle acceleration, Nature Photon. **3**(2009), 423–425

[3] *B. Y. Sharkov, D.H.H. Hoffmann et al.*, High energy density physics with intense ion beams, Matter and Radiation at Extremes **1**(2016), 28-47

[4] *M. Borghesi, A. Macchi, and G. S. Sarkisov*, Multi-MeV proton source investigations in ultraintense laser-foil interactions, Phys. Rev. Lett. **92**(2004), No. 5, 055003.

[5] V. N. Didenko et al., Contrast degradation in a chirped-pulse amplifier due to generation of prepulses by postpulses, Optics Express, **16**(2008), No. 5, 3178.

[6] *G. Honciuc et al.*, Antireflection coatings for high-power laser optics, High Power Laser Sci. Eng. **9**(2021), e43.

[7] *F. Quéré and H. Vincenti*, Reflecting petawatt lasers off relativistic plasma mirrors: A realistic path to the Schwinger limit, High Power Laser Sci. Eng.**9**(2021), e6.

[8] *T. Chapman et al.*, Investigation and modeling of optics damage in high-power laser systems caused by backscattered plasma", J. Appl. Phys. **3**(2019), No. 3, 033101.

[9] *Y. Cai et al.*, Time-resolved measurements on reflectivity of an ultrafast laser-induced plasma mirror, Phys. Plasmas **16**(2009), No. 10, 103104.

[10] *S. Ter-Avetisyan et al.*, Surface modulation and back reflection from foil targets irradiated by a Petawatt femtosecond laser pulse at oblique incidence, Opt. Express **24**(2016), No. 24, 28104-28112.

[11] *B. Dromey et al.*, The plasma mirror—A subpicosecond optical switch for ultrahigh power lasers, Rev Sci. Instrum. **75**(2004), No. 3, 645-649

[12] *A. Levy et al.*, Double plasma mirror for ultrahigh temporal contrast ultraintense laser pulses, Opt. Lett. **32**(2007), No. 3, 310

[13] *I.J. Kim et al.*, Spatio-temporal characterization of double plasma mirror for ultrahigh contrast and stable laser pulse", Appl. Phys. B" **104**(2011), No. 1, 81-86.

[14] *H. Vincenti et al.*, Optical properties of relativistic plasma mirrors, Nat. Commun. **5**(2014), 3403.

[15] *D. Kiefer*, Relativistic Electron Mirrors, Elsevier, 2015.

[16] *P. L. Poole et al.*Experiment and simulation of novel liquid crystal plasma mirrors for high contrast, intense laser pulses, Sci. Rep. **6**(2016), 32041.

[17] *H. Kiriyama et al.*, High-contrast high-intensity repetitive petawatt laser, Opt. Lett. **43**(2018), 2595.

[18] *J.-Y. Han et al.*Parametric geometry analysis for circular-aperture off-axis parabolic mirror segment, J. Astron. Telesc. Instrum. Syst. **5**(2019), No. 2, 024010.

[19] *B. Shi et al.*, Modified Frantz-Nodvik equation and numerical simulation of high-power innoslab laser amplifiers, Opt. Express **30**(2022), No. 10, 11026-11035.

[20] *I. Dancus et al.*, 10 PW Peak Power Laser at the Extreme Light Infrastructure Nuclear Physics – status updates, EPJ Web Conf. **266**(2022), 13008.

[21] *F. Lureau et al.*, High-energy hybrid femtosecond laser system demonstrating 2 × 10 PW capability, High Power Laser Sci. Eng. **8**(2020), e43.

[22] *K. Tanaka et al.*, Current status and highlights of the ELI-NP research program, Matter Radiat. Extrem. **5**(2020), No. 2, 024402.

[23] *D. Doria et al.*, Overview of ELI-NP status and laser commissioning experiments,J. Instr. **15**(2020), C09053.

[24] *S. Backus et al.*, High power ultrafast lasers, Rev. Sci. Instrum. **69**(1998), No. 3, 1207-1223.

[25] *F. L. Pedrotti, L. M. Pedrotti, and L. S. Pedrotti*, Introduction to Optics, 3rd Edition, Cambridge University Press, Cambridge, 2017.

[26] *A. A. Andreev et al.*, Backscattering of a high-intensity ultrashort laser pulse from a solid target at oblique incidence, Opt. Spectrosc. **102**(2007), No. 6, 944-948.

[27] https://www.azooptics.com/, "Step-by-Step Specifications to Design an Off-Axis Parabolic (OAP) Mirror".

[28] *M.O. Cernaianu et al.*, Commissioning of the 1 PW experimental area at ELI-NP using a short focal parabolic mirror for proton acceleration, Matter Radiat. Extremes **10**(2025), 027204.

[29] *O. Chalus et al.*, High-contrast 10 PW laser system at the Extreme Light Infrastructure - Nuclear Physics facility, High Power Laser Sci. Eng, **12**(2024), e90.